Available online at www.sciencedirect.com
ScienceDirect
Ceramics International 35 (2009) 2719–2725
CERAMICS INTERNATIONAL
www.elsevier.com/locate/ceramint

Preparation, characterization, spectral and conductivity studies of $Na_3MgZr(PO_4)_3$ and $Na_{0.1}(H_3O)_{2.9}MgZr(PO_4)_3$

B. Vijaya Kumar [a], Radha Velchuri [a], G. Prasad [b,*], M. Vithal [a]

[a] Department of Chemistry, Osmania University, Hyderabad - 500 007, India
[b] Department of Physics, Osmania University, Hyderabad - 500 007, India

Received 12 November 2008; received in revised form 29 January 2009; accepted 2 March 2009
Available online 27 March 2009

Abstract

$Na_3MgZr(PO_4)_3$ and $Na_{0.1}(H_3O)_{2.9}MgZr(PO_4)_3$ were prepared by microwave heating and ion exchange methods respectively. They were characterized by powder XRD, energy dispersive spectroscope (EDS), IR, Raman, TGA/DTA, DC conductivity and ^{31}P-MAS NMR spectra. These two compounds crystallized in the hexagonal NASICON lattice with $R\bar{3}c$ space group. The EDS spectra show the replacement of Na^+ by H_3O^+ ions. The infrared and Raman spectra exhibit characteristic vibrational bands of PO_4 tetrahedra and metal–oxygen vibrations. The DTA and TGA studies respectively indicate the structural phase transformations and absence of weight loss in these phosphates. The activation energies for conduction was found to be higher $Na_3MgZr(PO_4)_3$ compare to the value obtained for $Na_{0.1}(H_3O)_{2.9}MgZr(PO_4)_3$ and the values obtained are 0.41 and 0.082 eV (in the temperature range 27–165 and 165–360 °C) respectively. The DC conductivity of $Na_3MgZr(PO_4)_3$ is higher than the conductivity of $Na_{0.1}(H_3O)_{2.9}MgZr(PO_4)_3$. The conductivity values are found to be as $\sigma_{dc} = 1 \times 10^{-4}\ \Omega^{-1}\ cm^{-1}$ and $\sigma_{dc} = 1 \times 10^{-6}\ \Omega^{-1}\ cm^{-1}$at 250 °C respectively. The ^{31}P-MAS NMR spectra show the presence of two chemically different environments around phosphorous in these compounds.

Keywords: $Na_{0.1}(H_3O)_{2.9}MgZr(PO_4)_3$; Microwave heating; EDAX; ^{31}P-MAS NMR

1. Introduction

NASICON, an abbreviation for sodium (NA) super (S) ionic (I) conductor (CON), and related compounds have attracted the academic and industrial community since their discovery by Hong and Goodenough [1,2]. They are characterized by high ionic conductivity, low thermal expansion, high chemical stability, capacity to exhibit variation in the conductivity in the presence of guest molecules/ions and large surface area. The remarkable combination of properties of this class of materials has led to technological applications [3]. The chemical composition of NASICON is $Na_{1+x}Zr_2Si_xP_{3-x}O_{12}$ ($0 \leq x \leq 3$). Its 3D framework structure is characterized by corner sharing of ZrO_6 octahedra with PO_4 (or SiO_4) tetrahedra forming interconnected channels. It is generally represented as $AMM'(PO_4)_3$ and flexible for substitution at "A", "M", "M′" and "P" sites. The site "A" can also be vacant. The "A" ions occupy two different crystallographic sites: Type I sites (6b) situated between two MO_6 octahedra along the *c*-axis with a distorted octahedral coordination and Type II sites (18e) located between the ribbons (perpendicular to *c*-axis) with a trigonal prismatic coordination. The ribbons are connected by PO_4 tetrahedra along the *a*-axis [4]. The fast ionic conductivity of these materials is due to migration of sodium ions in the interconnected channels. Although sodium containing NASICONs are extensively studied, their protonated forms are scarcely reported despite their importance [5–9]. The ceramic NASICON type protonic conductors are useful in a variety of analytical/electrochemical applications due to their high ionic conductivities in the temperature range 293–373 K and used as a potentiometric or amperometric gas sensors. These materials could be used both as gas-impermeable membranes and as solid electrolytes in fuel cells, for producing hydrogen by electrolysis of steam or other gases, and for the electrolytic removal of hydrogen from air and gas streams [10–15]. To our knowledge, the spectral and conductivity studies of protonated form of $Na_3MgZr(PO_4)_3$ are not reported so far. The preparation and structure refinement of $Na_3MgZrP_3O_{12}$ is reported recently [16].

* Corresponding author: Tel.: +91 9440157980; fax: +91 040 27090020.
E-mail address: gudurup@gmail.com (G. Prasad).

0272-8842/$36.00
doi:10.1016/j.ceramint.2009.03.009

The present investigation deals with preparation, characterization, spectral and conductivity studies of $Na_3MgZr(PO_4)_3$ and $Na_{0.1}(H_3O)_{2.9}MgZr(PO_4)_3$ (here after referred to as NMZP and HMZP respectively).

2. Experimental

2.1. $Na_3MgZr(PO_4)_3$

The reported preparation consists of heating stoichiometric amounts of reactants at 750 °C for 24 h [16]. We have adopted microwave (MW) heating technique using a kitchen microwave oven. The stoichiometric amounts of NaH_2PO_4, $MgCO_3$ and $ZrO(NO_3)_2$ are thoroughly ground using spectral grade acetone and heated in a microwave oven operating at a frequency of 2.45 GHz for 5–7 cycles. Each cycle consists of heating for 1 min and cooling for 2 min. At the end of last cycle, the irradiation was terminated and the sample was allowed to cool inside the oven. The possible reaction is

$$3NaH_2PO_4 \cdot 2H_2O + MgCO_3 + ZrO(NO_3)_2 \xrightarrow{MW/5\,min} Na_3MgZr(PO_4)_3 + CO_2\uparrow + H_2O\uparrow$$

2.2. $Na_{0.1}(H_3O)_{2.9}MgZr(PO_4)_3$

About 2 g of $Na_3MgZr(PO_4)_3$ was taken in a round bottom flask and reflected (a) once with 0.2 mol/L HCl for 6–8 h and (b) five times in fresh solution of 1 mol/L HCl for 24 h. Each time 10 ml of HCl per 1 g of powder is taken. The solid obtained at the end of final reflection was washed with distilled water and dried at 90 °C. The filtrate obtained at each stage is mixed and slowly evaporated to dryness. The solid obtained after evaporating the filtrate was identified as NaCl.

The compositional analysis was carried out by HITACHI Model S-3500H scanning electron microscope (SEM) equipped with a Horiba EMAX-ENERGY energy dispersive spectroscope (EDS).

Powder X-ray diffractograms were collected using Philips X pert analytical X-ray diffractometer. Nickel filtered Cu-Kα radiation of wavelength 1.5406 Å. XRD pattern were indexed and lattice parameters were calculated using POWDX program. Experimental densities were measured by Archimedes principle using xylene as an immersion liquid. Calculated densities were obtained from lattice parameters.

Infrared spectra are recorded in the form of KBr pellets in the wave number range 4000–400 cm^{-1} using JASCO IR-5300 spectrometer and the Raman spectra are recorded on RENISHAW 1000B spectrometer in the wave number range 100–1500 cm^{-1}. The laser wavelength and its output are 532 nm and 5 mW respectively.

TGA/DTA of powder samples was carried out on Mettler Toledo TGA/SDTA-851_e model in nitrogen atmosphere in the temperature region 25–200 °C at the rate of 5 °C min^{-1}.

The ^{31}P solid state MAS NMR spectra were recorded with a Bruker DSX-300 MHz high resolution spectrometer operating at 121.49 MHz with 7.45 kHz spinning speed. The samples were packed in a 4-mm Zirconia rotor. Pulses of 90° with 4.2 μs duration were employed with a recycle delay of 5 s between pulses and the spectra were recorded at room temperature. The chemical shift values are given with respect to an 85% H_3PO_4 solution.

The DC conductivities are measured in the temperature range 30–350 °C using a two probe method on the sintered pellets coated with silver paint. The ceramic pellets used for the conductivity measurements have about 2% porosity. For this a conventional sample holder and Keithley Electrometer 610C are used.

3. Results and discussions

3.1. EDS analysis

The energy dispersive spectra of NMZP and HMZP are recorded to confirm the replacement of Na^+ ions by H^+ ions (in the form of H_3O^+). As shown in Fig. 1, the intensity of sodium peak at 1.1 keV in the HMZP sample is about 3% compared to the sodium peak in NMZP sample indicating that about 97% of Na^+ ions are replaced by H^+ ions. The molecular formula of protonated form of NMZP can be written as $Na_{0.1}[H(-H_2O)_n]_{2.9}MgZr(PO_4)_3$, where n may be equal to one or more than one.

3.2. Powder XRD

Fig. 2 shows the powder X-ray diffractograms of NMZP and HMZP. The observed *d*-lines of NMZP were similar to those reported [16] while the *d*-lines of HMZP were similar to that of NMZP. These powder XRDs correspond to a single phase

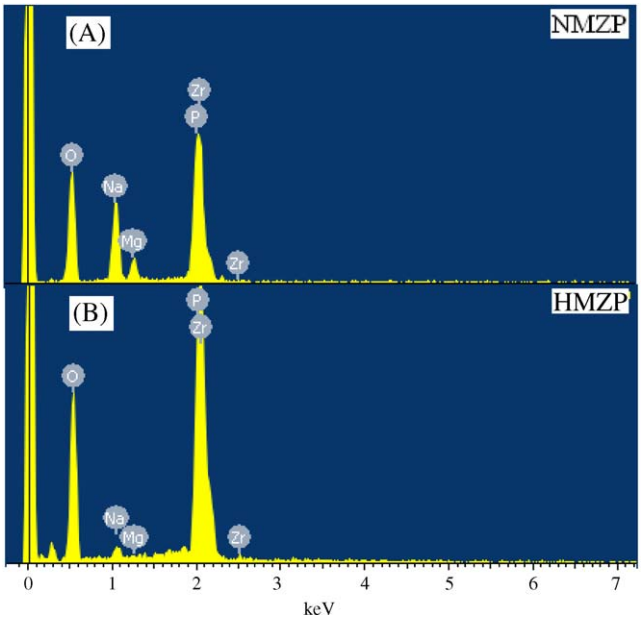

Fig. 1. EDS of (A) $Na_3MgZr(PO_4)_3$ and (B) $Na_{0.1}(H_3O)_{2.9}MgZr(PO_4)_3$.

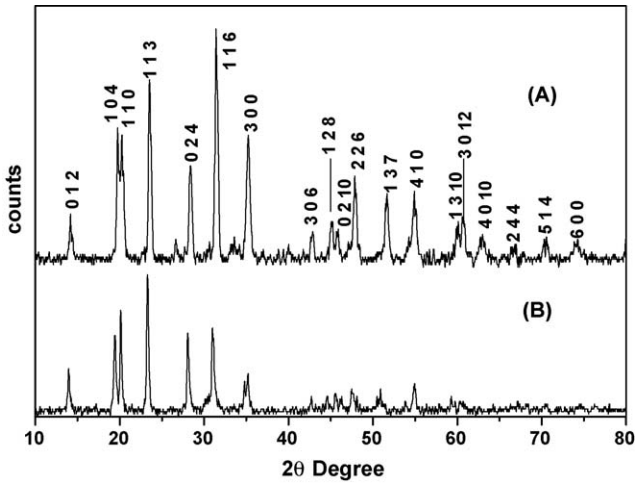

Fig. 2. XRD patterns of (A) $Na_3MgZr(PO_4)_3$ and (B) $Na_{0.1}(H_3O)_{2.9}MgZr(PO_4)_3$.

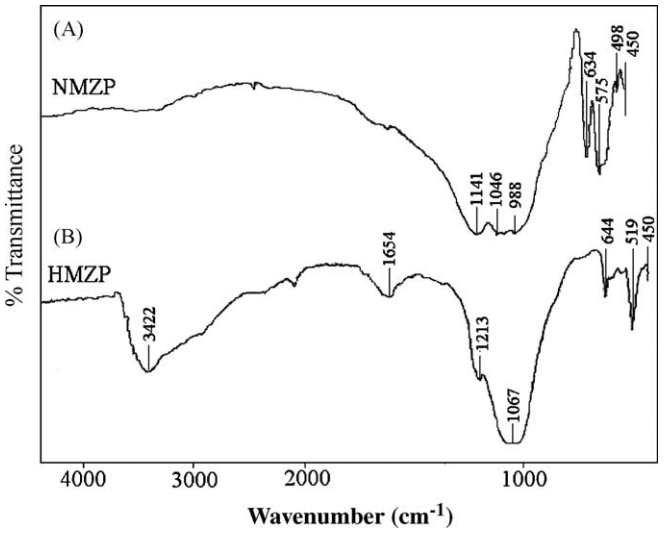

Fig. 3. IR spectra of (A) $Na_3MgZr(PO_4)_3$ and (B) $Na_{0.1}(H_3O)_{2.9}MgZr(PO_4)_3$.

belonging to NASICON family with no detectable impurity. It is well known that the type of lattice adopted by NASICON type compounds depends on the composition and experimental conditions [17–19]. These materials crystallize in either hexagonal or monoclinic lattice [20]. The monoclinic phase belonging to NASICON family is characterized by the observation of *d*-lines at $2\theta = 13–17^\circ$ and at $2\theta = 21$, 22, 25, 31, 34. The absence of *d*-lines at these positions in HMZP suggests that it is crystallized in hexagonal lattice The unit cell parameters of HMZP are calculated by using the least square fit program, POWD, by taking the unit cell parameters of the reported compound $Na_3MgZr(PO_4)_3$ as input parameters [16]. The unit cell parameters thus obtained are given in Table 1 along with the unit cell parameters of NMZP. The powder XRD of HMZP and its unit cell parameters suggest that it is isomorphous with NMZP. Chakir et al. have reported that sodium ions in NMZP were distributed into M1 and M2 sites anisotropically [16]. Such a distribution of H_3O^+ ions may also exist in HMZP which is supported by IR/Raman and ^{31}P-MAS NMR results. The experimental densities along with the theoretical values obtained from unit cell parameters are also given in Table 1.

3.3. IR and Raman spectra

Fig. 3 gives the infrared spectra of NMZP and HMZP. The spectral features observed in the region 1500–400 cm^{-1} are similar for both the compositions. However, broad bands at 3422 and 1654 cm^{-1} were observed for HMZP which were absent in the case of NMZP. The broad bands at 3422 and 1654 cm^{-1} are known to be due to O–H stretching [ν(OH)] and H–O–H bending [ν (H–O–H)] vibrations of H_3O^+ [21,22]. The presence of O–H band in the sample could be due to (i) H_3O^+ or (ii) H^+ $(H_2O)_n$ ($n > 1$) as it was reflected with dilute HCl. Colomban et al. have reported the infrared spectra of H_3O^+ β-alumina and H^+ $(H_2O)_n$ β-alumina ($n > 1$) based on the number and positions of O–H stretching vibrations. It was noticed that (H_3O^+) β-alumina gives only one broad band in the region 3100–3300 cm^{-1} while H^+ $(H_2O)_n$ β-alumina ($n > 1$) gives broad bands at (i) 3380 (ii) 2900 and (iii) 2540 cm^{-1} [22]. In the present investigation, we have observed only one broad band at 3422 cm^{-1}.Therefore the composition of the hydrated form of NMZP can be written as $Na_{0.1}(H_3O)_{2.9}(PO_4)_3$. Further, the infrared spectrum of HMZP heated to 200 °C/24 h was found to be similar to that shown in Fig. 3 indicating the chemical stability of $Na_{0.1}(H_3O)_{2.9}MgZr(PO_4)_3$. The spectral features observed below 1500 cm^{-1} can be assigned to internal and external modes of PO_4 tetraherda and lattice modes. It is observed that phosphate group vibrations are strong compared to the lattice modes and metal–oxygen vibrations. According to factor group analysis, nine vibrational modes are expected for PO_4 group [23–25]. They are (i) the symmetric non degenerate (ν_1) PO stretching observed in the range 950–1070 cm^{-1}; (ii) asymmetric doubly degenerate (ν_2) PO stretching observed at 440–450 cm^{-1}; (iii) symmetric triply degenerate (ν_3) OPO bending observed at 1100–1160 cm^{-1} and (iv) triply degenerate asymmetric and harmonic OPO bending (ν_4) observed at 545–680 cm^{-1}. The observed IR and Raman bands for both the samples and their assignments are represented in Table 2.

Table 1
Unit cell parameters and densities of NMZP and HMZP.

Compound	Lattice parameters		Density		Volume (Å^3)
	a (Å)	*c* (Å)	d_{obs} (g cm^{-3}) ±0.02	d_{cal} (g cm^{-3}) ±0.02	
$Na_3MgZr(PO_4)_3$	8.884	22.554	3.10	3.03	1541
$Na_{0.1}(H_3O)_{2.9}MgZr(PO_4)_3$	8.860	22.89	2.62	2.58	1556

Table 2
Raman and IR band positions (in cm^{-1}) of NMZP and HMZP along with their assignments.

$Na_3MgZr(PO_4)_3$				$Na_{0.1}(H_3O)_{2.9}MgZr(PO_4)_3$
Raman	IR	Raman	IR	Approximate type of motion
–	–	–	3442	ν(O–H)
–	–	–	1654	ν(H–O–H)
1220	–	–	1213	$\nu_3(PO_4)$
1117	–	–	–	
1029	1046	1025	1067	
970	988	–	–	$\nu_1(PO_4)$
632	634	637	644	$\nu_4(PO_4)$
593	–	613	–	
561	575	534	519	
479	498	474	–	$\nu_2(PO_4)$
431	450	422	450	
317	–	379	–	ν(M–O)
255	–	291	–	

The Raman spectrum of HMZP, shown in Fig. 4, was found to be similar to that reported for NMZP except for small variation in intensity [16]. All the peaks observed in the region 200–1300 cm^{-1} are found to be relatively broad compared to the Raman spectrum of $NaZr_2(PO_4)_3$ [23]. The broadness of Raman lines in NASICON type materials is related to relative chemical environment and symmetry of PO_4 tetrahedra [16]. In the case of $NaZr_2(PO_4)_3$, sodium ions occupy M1 site completely and M2 sites are vacant [26]. The PO_4 unit in $NaZr_2(PO_4)_3$ is surrounded by ZrO_6 and $Na(1)O_6$ units only. Thus the PO_4 unit in $NaZr_2(PO_4)_3$ is in relatively symmetric environment and gave rise to sharp Raman lines. In the case of HMZP, on the other hand, the PO_4 unit is linked to ZrO_6, MgO_6, $H_3O(1)O_6$ and $H_3O(2)O_8$ units which is relatively disordered compared to PO_4 unit in $NaZr_2(PO_4)_3$ and hence gave rise to relatively broad Raman spectra.

3.4. TGA/DTA analysis

The TGA and DTA profiles of NMZP and HMZP are shown in Figs. 5 and 6 spectively. The TGA of NMZP and HMZP did not exhibit any significant weight loss in the temperature range 40–240 °C. It is observed that materials possessing H_3O^+ group are stable up to 400–500 °C [22]. In the present investigation, the weight loss up to 240 °C was found to be negligible (<0.5%) indicating the absence of trapped water in the channels of lattice and since H_3O^+ is reported to be stable even up to about 500°C these ions are present in the samples as

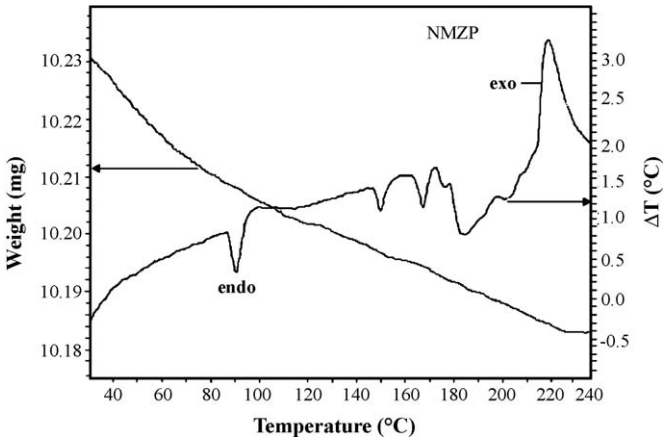

Fig. 5. TG/SDTA curves of $Na_3MgZr(PO_4)_3$.

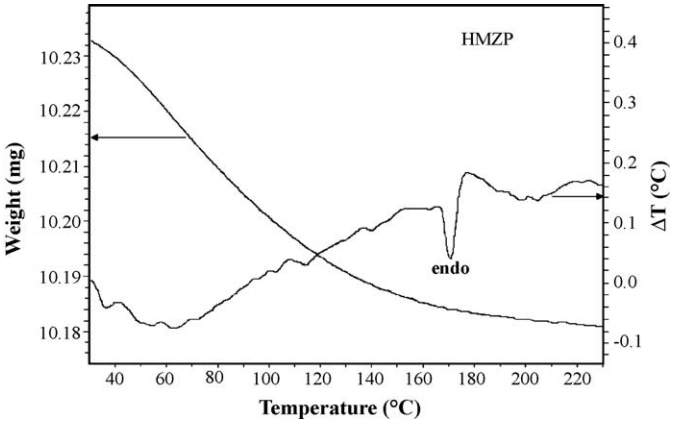

Fig. 6. TG/SDTA curves of $Na_{0.1}(H_3O)_{2.9}MgZr(PO_4)_3$.

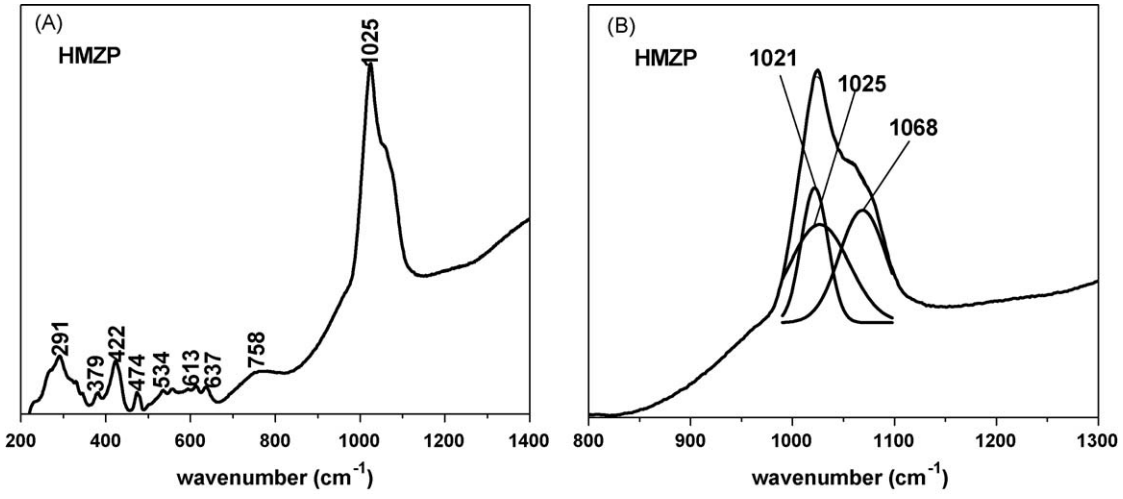

Fig. 4. Raman spectra of $Na_{0.1}(H_3O)_{2.9}MgZr(PO_4)_3$ in the range (A) 200–1400 cm^{-1} and (B) 800–1300 cm^{-1} with Gaussian fitting.

discussed earlier. This result is in congruent with infrared results discussed earlier. The DTA of NMZP shows (i) endothermic peaks at 90, 150, 170–180 °C and (ii) exothermic peak at 210–240 °C while the DTA of HMZP shows one endothermic peak centered in the temperature range 170–180 °C. These peaks may be attributed to structural phase transformations as NASICON type materials are known to crystallize in more than one type of lattice [20]. The resistivity measurements also exhibit changes in slopes at these temperatures.

3.5. DC conductivity

The variations of σ_{dc} T with inverse temperature, where σ_{dc} is DC conductivity obtained from the bulk resistance and sample dimensions for the NMZP and HMZP are presented in Fig. 7. The variation of conductivity of NMZP with temperature is interesting. The conductivity was found to be linear in the regions (a) 27–97 °C and (b) 140–250 °C. The slopes of these two linear regions were, however, different. The conductivity was found to increase with increase in temperature in these two regions. In the temperature region, 97–140 °C, the conductivity was found to marginally decrease with increase in the temperature. The observed marked change in the conductivity at 97 and 140 °C may be attributed to structural phase transformations. The DTA curve of NMZP also shows phase transformations at 90 and 150 °C. Thus both DTA and conductivity results confirm structural phase transformations (Fig. 8).

The variation of conductivity of HMZP also exhibits an interesting feature. The variation of conductivity with temperature exhibits two linear regions viz., (a) 27–165 °C and (b) 165–350 °C. A change in the slope is noticed at 165 °C. This temperature is close to the endothermic peak temperature (170 °C) observed in its DTA curve. Thus HMZP also undergoes a structural phase transformation at this temperature.

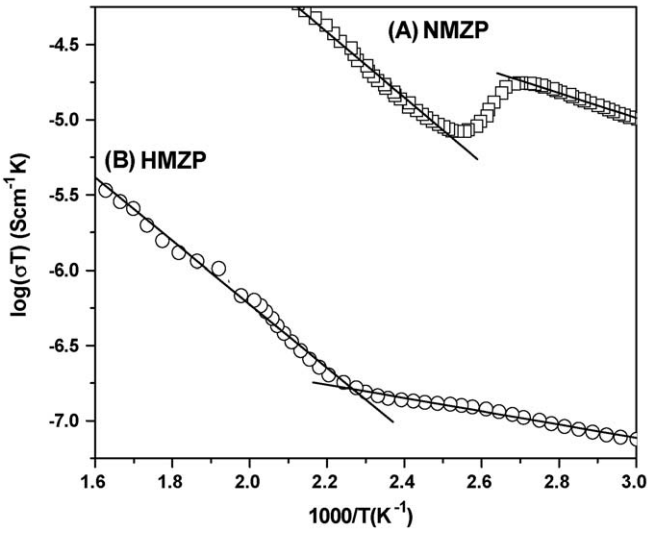

Fig. 7. DC conductivity plot of (A) $Na_3MgZr(PO_4)_3$ and (B) $Na_{0.1}(H_3O)_{2.9}MgZr(PO_4)_3$.

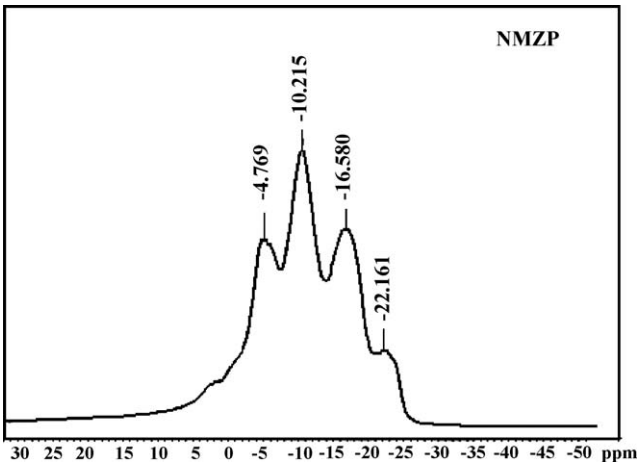

Fig. 8. Solid state ^{31}P-MAS NMR spectrum of $Na_3MgZr(PO_4)_3$.

The conductivity follows the Arrhenius behavior of the form:

$$\sigma_{dc}T = \sigma_0 \exp(-E_a/kT)$$

where σ_0 is the pre-exponential factor, T is the absolute temperature, E_a is the activation energy for conduction and k is the Boltzmann's constant. The observed conductivities of HMZP at 250 °C is $\sigma_{dc} = 1\times10^{-6}\ \Omega^{-1}\ cm^{-1}$ and NMZP is $\sigma_{dc} = 1 \times 10^{-4}\ \Omega^{-1}\ cm^{-1}$. The activation energies (E_a(dc)) for conduction of NMZP found to be (0.42 eV in the temperature range 27–97 °C) and 0.17 eV (in the region 130–250 °C). Similarly the activation energies of HMZP were 0.41 and 0.082 eV in the temperature range 27–165 and 165–360 °C respectively.

The conductivity of NASICON type compounds in general increases with increase in temperature. The ionic nature of Na–O bond and the easy movement of Na^+ ions in the channels of skeletal hexagonal lattice are mainly responsible for high conductivity in these NASICON type compounds. In the case of NMZP, in the temperature regions 27–97 °C and 135–250 °C this trend is observed. However, in the temperature region 97–135 °C a marginal decrease in conductivity was noticed. This decrease in conductivity may be due to structural phase transformation such that the channels in the skeletal lattice are partially affected hindering the movement of Na^+ ions. The conductivity of NMZP at any given temperature was more than that of HMZP. The larger conductivity of NMZP could be due to more ionic nature of O–Na bond in the NASICON framework compared to O–H bond (the electronegativity difference between Na and O is 2.6 while the electronegativity difference between H and O is 1.2) and/or smaller size of Na^+ compared to that of H_3O^+ [15].

3.6. Solid state ^{31}P-MAS NMR

The ^{31}P-MAS NMR of NMZP and HMZP were recorded to find the local structure of phosphorous ions in these NASICON architectures. It is well known that ^{31}P-MAS NMR gives different signals for chemically/crystallographically inequiva-

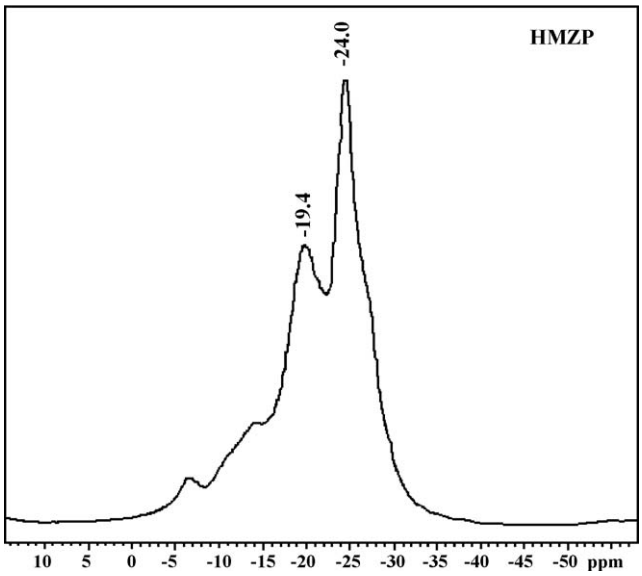

Fig. 9. Solid state ^{31}P-MAS NMR spectrum of $Na_{0.1}(H_3O)_{2.9}MgZr(PO_4)_3$.

lent sites of phosphorous. For instance the ^{31}P-MAS NMR spectra of $NaZr_2(PO_4)_3$ and $LiTi_2(PO_4)_3$ gave only one symmetric peak and all the phosphorous atoms occupy at only one site at 18e position of the hexagonal lattice with $R\bar{3}c$ space group [27]. On the other hand, two peaks were observed in $Na_5Ti(PO_4)_3$ suggesting the occupation of phosphorous at two crystallograhically different sites [27]. The ^{31}P-MAS NMR of NMZP and HMZP are shown in Fig. 9 and 10 respectively. The ^{31}P-MAS NMR of NMZP shows prominent peaks at −10.2 and −16.6 ppm with shoulders indicating the presence of phosphorous in at least two chemically/ crystallographically different environments. As the sodium ions are distributed into M1 and M2 sites anisotropically, the phosphorous atoms are likely to be surrounded by (a) ZrO_6, MgO_6, $Na(1)O_6$ and (b) ZrO_6, MgO_6, $Na(2)O_8$ units giving rise to two NMR peaks. The ^{31}P-MAS NMR of HMZP exhibits two peaks at −19.4 (with small shoulders) and −24 ppm. These chemical shift values are different from chemical shift values of NMZP indicating the exchange of Na^+ by H_3O^+ ions. The presence of two peaks in HMZP again confirm the distribution of H_3O^+ ions into M1 and M2 sites anisotropically giving rise to two chemically different environments around phosphorous. The chemical shift values of NMZP and HMZP are given in Table 3 along the $NaZr_2(PO_4)_3$, $LiZr_2(PO_4)_3$, $Na_5Zr(PO_4)_3$ and $Na_5Ti(PO_4)_3$ for a comparison.

Table 3
Chemical Shifts for the NMZP and HMZP along with other related compounds.

Composition	Chemical shift (ppm)	Reference
$Na_3MgZr(PO_4)_3$	−10.2, −16.6	Present work
$Na_{0.1}(H_3O)_{2.9}MgZr(PO_4)_3$	−24.0, −19.4	Present work
$NaZr_2(PO_4)_3$	−24.3	[27]
$LiTi_2(PO_4)_3$	−26.2	[27]
$Na_5Zr(PO_4)_3$	−2.0, −6.6	[27]
$Na_5Ti(PO_4)_3$	0.5, −5.0	[27]

4. Conclusions

NMZP and HMZP were prepared and characterized by powder XRD, EDS, IR, Raman, TGA/DTA, ^{31}P-MAS NMR and DC conductivity. HMZP was found to crystallize in hexagonal lattice and isomorphous with NMZP. The infrared and Raman spectra exhibit characteristic vibrational bands due to PO_4 tetrahedra and metal–oxygen vibrations. Both NMZP and HMZP undergo structural phase transformations below 240 °C. The TGA profiles exhibit absence of weight loss. The DC conductivity of NMZP exhibits irregular variation with temperature while the DC conductivity of HMZP shows linearity with temperature albeit with a change in slope. The reasons for such irregular variation are given. The DC conductivity of NMZP was higher than the conductivity of HMZP due to ionic nature of Na–O. The ^{31}P-MAS NMR spectra of NMZP and HMZP suggest at least two chemically different environments around phosphorous.

Acknowledgement

The authors sincerely thank the referees for helpful suggestions and Department of Science and Technology (DST) for financial support.

References

[1] H.Y.P. Hong, Crystal structures and crystal chemistry in the system $Na_{1+x}Zr_2Si_xP_{3-x}O_{12}$, Mater. Res. Bull. 11 (1976) 173–182.
[2] J.B. Goodenough, H.Y.P. Hong, J.A. Kafalas, Fast Na^+-ion transport in skeleton structures, Mater. Res. Bull. 11 (1976) 203–220.
[3] P. Padma Kumar, S. Yashonath, Ionic conduction in the solid state, J. Chem. Sci. 118 (2006) 135–154.
[4] L.O. Hagmann, P. Kierkegaard, The crystal structure of $NaMe_2^{IV}(PO_4)_3$, Me^{IV} = Ge, Ti, Zr, Acta. Chem. Scand. 22 (1968) 1822–1832.
[5] J. Gulens, B.W. Hildebrandt, J.D. Canaday, A.K. Kuriakose, T.A. Wheat, A. Ahmad, Influence of water on the electrochemical response of a bonded Nasicon protonic conductor, Solid State Ionics 35 (1989) 45–49.
[6] P. Colomban, Proton Conductors: Solids, Membranes and Gels—Materials and Devices, Cambridge University press, 1992(chapter 15, 224–237).
[7] M.A. Subramanian, B.D. Roberts, A. Clearfield, On the proton conductor $(H_3O)Zr_2(PO_4)_3$, Mat. Res. Bull. 19 (1984) 1471–1478.
[8] P.R. Rudolf, M.A. Subramanian, A. Clearfield, J.D. Jorgensen, The crystal structure of the ion conductors $(NH^+_4)Zr_2(PO_4)_3$ and $(H_3O^+)Zr_2(PO_4)_3$, Solid State Ionics 17 (1985) 337–342.
[9] A. Clearfield, Structural concepts in inorganic proton conductors, Solid State Ionics 46 (1991) 35–43.
[10] S. Konishi, H. Ohno, H. Yoshida, H. Katsuta, Y. Naruse, Solid oxide electrolysis cell for decomposition of tritiated water, Int. J. Hydrogen Energy 11 (1986) 507–512.
[11] S.F. Chehab, J.D. Canaday, A.K. Kuriakose, T.A. Wheat, A. Ahmad, A hydrogen sensor based on bonded hydronium NASICON, Solid State Ionics 45 (1991) 299–310.
[12] N. Maffei, A.K. Kuriakose, A hydrogen sensor based on conducting solid electrolyte, Sens. Actuat. B 56 (1999) 243–246.
[13] M. Kleitz, P. Fabry, J.F. Millon-Brodaz, E. Siebert-Mantel, Solid state ionics for advanced chemical sensors, Solid State Ionics 18 (19) (1986) 98–100.
[14] N. Maffei, A.K. Kuriakose, A solid-state potentiometric sensor for hydrogen detection in air, Sens. Actuat. B 98 (2004) 73–76.
[15] J. Gulens, T.H. Longhurst, A.K. Kuriakose, J.D. Canaday, Hydrogen electrolysis using a Nasicon solid protonic conductor, Solid State Ionics 28 (30) (1988) 622–626.

[16] M. Chakir, A. El Jazouli, D. de Waal, Synthesis, crystal structure and spectroscopy properties of $Na_3AZr(PO_4)_3$ (A = Mg, Ni) and $Li_{2.6}Na_{0.4}$-$NiZr(PO_4)_3$ phosphates, J. Solid State Chem. 179 (2006) 1883–1891.

[17] G. Collin, R. Comes, J.P. Boilot, Ph. Colomban, Disorder of tetrahedral in Nasicon-type structure—I. $Na_3Sc_2(PO_4)_3$: structures and ion–ion correlations, J. Phys. Chem. Solids 47 (1986) 843–854.

[18] G. Collin, R. Comes, J.P. Boilot, Ph. Colomban, Nasicon analog $Na_3Sc_2(PO_4)_3$: thermal behaviour of the α, β and γ types, structure, correlations and transitions, Solid State Ionics 28 (30) (1988) 437–441.

[19] J.P. Boilot, G. Collin, Ph. Colomban, Relation structure-fast ion conduction in the NASICON solid solution, J. Solid State Chem. 73 (1988) 160–171.

[20] K. Kasturi Rangan, J. Gopalakrishnan, $AM^{V}M^{III}(PO_4)_3$: new mixed-metal phosphates having NASICON and related structures, Inorg. Chem. 34 (1995) 1969–1972.

[21] K. Nakamoto, Infrared and Raman Spectra of Inorganic and Coordination Compounds, Part I: Theory and Applications in Inorganic Chemistry, Wiley, New York, 1997p.159.

[22] Ph. Colomban, G. Lucazeau, R. Mercier, A. Novak, Vibrational spectra and structure of $H^+(H_2O)_n$ β-alumina, J. Chem. Phys. 67 (1977) 5244–5251.

[23] M. Barj, H. Perthuis, Ph. Colomban, Domaines d'existence distorsions structurales et modes de vibration des ions conducteurs dans les reseaux hotes de type Nasicon, Solid State Ionics 11 (1983) 157–177.

[24] A. Mbandza, E. Bordes, P. Courtine, Preparation and structural properties of the solid state ionic conductor $CuTi_2(PO_4)_3$, Mat. Res. Bull. 20 (1985) 251–257.

[25] G. Le Polles, J.-J. Videau, R. Olazcuaga, Analyse Structurale par Spectroscopie Raman et Infrarouge de Quelques phosphates de Cuivre de Type Nasicon, J. Solid State Chem. 127 (1996) 341–349.

[26] M. Barj, G. Lucazeau, C. Delmas, Raman, Infrared spectra of some chromium Nasicon-type materials: short-range disorder characterization, J. Solid State Chem. 100 (1992) 141–150.

[27] K.C. Sobha, K.J. Rao, ^{31}P MAS NMR investigations of crystalline and glassy NASICON-type phosphates, J. Solid State Chem. 121 (1996) 197–201.